

<https://doi.org/10.1038/s42005-025-02109-x>

Dynamics of a helical vortex ring interacting with a vortex line

Wen-Kai Bai^{1,2}, Xue Yang¹, Hao Zhu², S. A. Gardiner³✉, Wu-Ming Liu²✉ & Tao Yang^{1,4}✉

Helical vortex rings are intriguing flow phenomena observed in both classical and quantum fluids, playing a crucial role in the examination of turbulence. Despite significant research dedicated to understanding their dynamics, studies on the interaction between vortex lines and vortex rings remain limited. Here, we show the dynamics of a helical vortex ring interacting with a vortex line. Through manipulation of the polarity and magnitude of the topological charge along the axis of the vortex ring, we show a change in the translational speed and angular rotation of the vortex ring. To gain deeper insights into the dynamics of intricate vortex structures in the presence of a vortex line, we analyse the evolution of the moment of inertia tensor during this evolution. The results provide insights into the dynamics of helical vortex rings, contributing to a deeper comprehension of turbulence generation and dissipation.

Vortices are a fascinating and extensively studied phenomenon in various classical and quantum systems, such as water^{1–3}, air^{4,5}, optics^{6,7}, and Bose–Einstein condensates (BECs)^{8–10}. They can take the form of vortex lines, vortex knots, and vortex links in three-dimensional (3D) space^{11–14}. Among these, vortex rings, the simplest knots in topology, have attracted significant attention due to their association with exotic phenomena^{15–17}. BECs offer an ideal platform for investigating the quantum dynamics of topological excitations due to their clean and controllable properties. In contrast, in a classical medium, phenomena such as emission and reconnection are significantly affected by environmental noise, posing significant challenges in understanding the fundamental mechanisms. Moreover, stable vortex rings have been successfully produced in two-component BECs through the disintegration of dark solitons¹⁸. Furthermore, individual vortex rings display periodic oscillations in confined BECs¹⁹.

Helical vortex rings are commonly considered to be perturbed vortex rings influenced by Kelvin waves, which cause the vortex core to deviate from its ideal rotationally symmetric shape and take on a helical displacement. The movement of a helical vortex ring can be broken down into translation and rotation. While there has been extensive research on the translational speed, the properties of the rotation remain uncertain. Generally, the presence of helical waves inhibits the translational speed of vortex rings and may result in a reversal of their direction of motion^{20,21}. This phenomenon is associated with the conservation of angular momentum within the flow surrounding the axis of the ring. Experimental studies have observed the rotation of vortex rings in water using fluorescent dye visualization to observe the illumination pattern²². The inherent angular speed

can be analytically calculated by taking the partial derivative of the vortex ring's energy with respect to the angular momentum along the ring axis²¹. Kelvin waves can induce perturbations that enable the connection of vortex rings to form intricate vortex structures, including knots and links²³.

The interaction between vortex rings and vortex lines is a fascinating and engaging problem in the field of vortex dynamics. Their mutual influence gives rise to intriguing phenomena, such as the formation of vortex hopfions, in which the vortex line typically lies on the axis of the vortex ring. The stability of hopfions is significantly influenced by their interaction^{24–27}. Additionally, the interaction and reconnection of vortex rings and vortex lines play a critical role in the dissipation of vortex tangles, making them a focal point in the study of turbulence. The decay of Kolmogorov quantum turbulence proceeds through the Kelvin wave cascade process, involving the nonlinear interactions of Kelvin waves along quantized vortex lines. This cascade leads to the generation of progressively shorter Kelvin wave wavelengths until they are capable of effectively emitting sound²⁸. In contrast, ultra-quantum turbulence decay can occur in regions of high curvature on vortex lines, where vortex reconnection is triggered when local curvature surpasses a critical threshold, resulting in the release of vortex rings^{29–31}. Understanding the dynamics and behavior of vortex rings and vortex lines is of utmost importance in unraveling the complexities of turbulence^{32–35}.

In this study, we explore the dynamics of helical vortex rings in trapped BECs by numerically solving the Gross–Pitaevskii (GP) equation. Our investigation revealed that both the translational and rotational dynamics of a helical vortex ring are influenced not only by helical waves but also by a

¹Shaanxi Key Laboratory for Theoretical Physics Frontiers, Institute of Modern Physics, Northwest University, Xi'an, 710127, China. ²Beijing National Laboratory for Condensed Matter Physics, Institute of Physics, Chinese Academy of Sciences, Beijing, 100190, China. ³Joint Quantum Centre (JQC) Durham-Newcastle, Department of Physics, Durham University, Durham, DH1 3LE, UK. ⁴Peng Huanwu Center for Fundamental Theory, Xi'an, 710127, China.

✉ e-mail: s.a.gardiner@durham.ac.uk; wliu@iphy.ac.cn; yangt@nwu.edu.cn

central vortex line. We observe that the increase in translational speed is modulated by the topological charge of the vortex line. Additionally, we expand our analysis to include more complex vortex structures, such as trivial links and trefoil knots, in order to investigate their dynamic behavior. Furthermore, we find that certain aspects of vortex dynamics can be accurately characterized by calculating the moment of inertia tensor, which offers additional insights into their behavior.

Results and discussion

Model

At sufficiently low temperatures, the dynamics of 3D BECs can be described by the time-dependent GP equation,

$$i\hbar \frac{\partial \psi}{\partial t} = \left(-\frac{\hbar^2}{2m} \nabla^2 + V_{\text{trap}} + g|\psi|^2 \right) \psi, \quad (1)$$

where ψ represents the complex wave function, and V_{trap} is a cylindrical box potential (see Eq. (5) in Method). Here, $g = 4\pi\hbar^2 a_s/m$ is the coupling constant, with a_s being the s-wave scattering length. For convenience, all units in the following are dimensionless (see “Methods” for dimensionless process and initial state construction). The intrinsic translational speed of an ideal vortex ring moving within a homogeneous condensate can be described by $v_r = \hbar / (2mR_r) [\ln(8R_r/\xi) - 0.615]$, where $\xi = 1/\sqrt{8\pi\rho a_s}$ represents the healing length and R_r represents the radius of the ring³⁶. However, in practical scenarios, vortex rings are rarely circular due to the influence of Kelvin waves, which play a crucial role in understanding turbulence mechanisms³⁷. In such cases, a more comprehensive characterization of the dynamics of vortex rings can be achieved by calculating the z-component of

the center of mass of the ring³⁸

$$z_{\text{cm}} = \frac{\int_V z (\rho_{\text{th}} - |\psi|^2) H[\rho_{\text{th}} - |\psi|^2] dV}{\int_V (\rho_{\text{th}} - |\psi|^2) H[\rho_{\text{th}} - |\psi|^2] dV}, \quad (2)$$

where $H[\dots]$ represents the Heaviside step function, and ρ_{th} corresponds to a threshold value of density isosurface. In addition to the method mentioned above for calculating the center of mass, the center of mass can also be determined using the “plaquette” technique, which involves identifying the vortex core position by detecting the 2π phase winding³⁹.

Vortex ring translational speed

In Fig. 1a, we illustrate the density isosurface of a vortex ring combined with an $s=4$ vortex line (the green tube). The gray ring shows the original position. The corresponding speed field is shown in Fig. 1b. The translational speed of the vortex ring in the presence and absence of a central vortex line is represented by v_{rl} and v_{r_0} , respectively. The increase in the relative speed, denoted by v_{rl}/v_{r_0} as a function of the topological charge s , can be observed in Fig. 1d with respect to different radii R_r of the vortex ring. Importantly, the direction of the circulation field induced by the vortex rings remains perpendicular to the direction of the speed field induced by the vortex line, regardless of the sign of the topological charge (for example $s=\pm 1$). Therefore, v_{rl} does not change with the sign of the topological charge. The key parameters in this scenario are the radius of the vortex ring R_r and the absolute value of the topological charge $|s|$ carried by the vortex line. In Fig. 1e, v_{rl}/v_{r_0} is shown as a function of R_r for different s . It is evident that a larger topological charge of the vortex line combined with a smaller radius of the vortex ring can lead to a higher translational speed of the vortex ring.

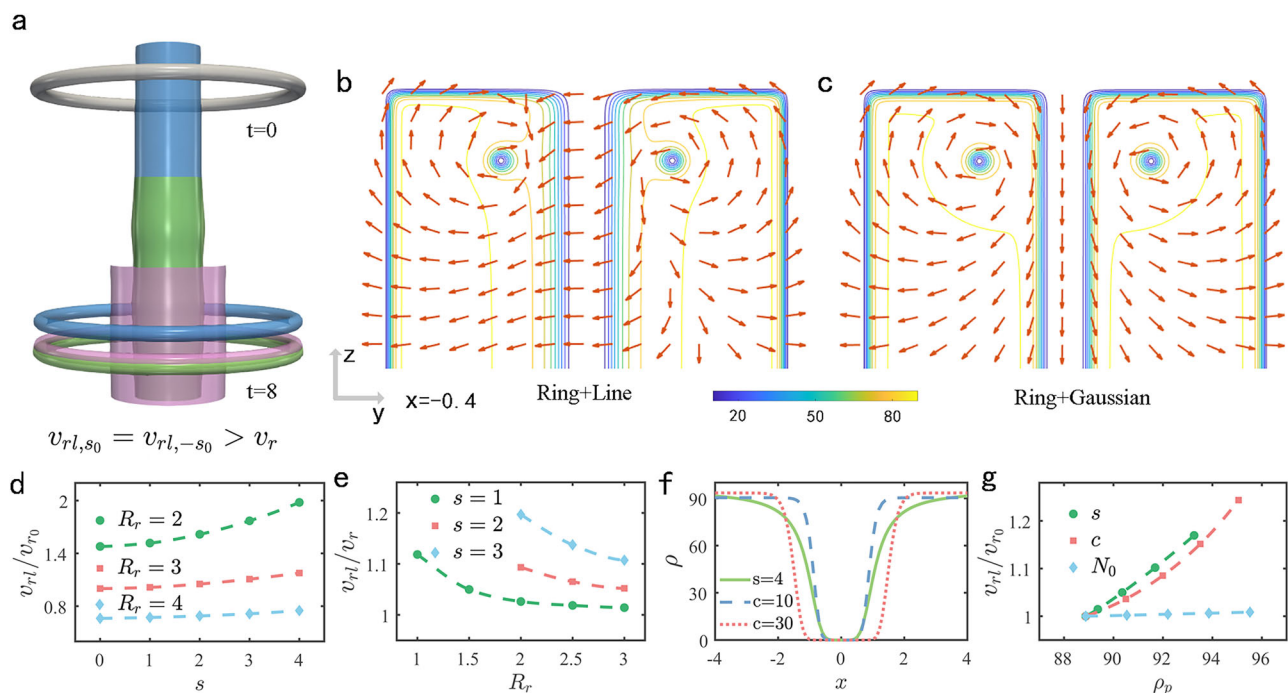


Fig. 1 | Translational dynamics of vortex rings. **a** The gray ring indicates the density isosurface of the vortex ring with the radius $R_r = 3$ at time $t = 0$ for all cases. The green tube is the density isosurface of the vortex ring with the topological charge $s = 4$. The blue tube and pink tube are the density isosurfaces of the density hole created by the Gaussian impurities with the half-width $c = 10$ and $c = 30$, respectively. The green ring is the position of the vortex ring moving along the vortex line at $t = 8$. The blue ring and the pink ring indicate the positions of the vortex rings moving along the corresponding Gaussian impurities at $t = 8$, respectively. **b, c** The corresponding speed fields are shown for the vortex ring in the presence of a vortex line with $s = 4$ and for the vortex ring in the presence of a Gaussian impurity with

$c = 10$, respectively. **d** Relative translational speed v_{rl}/v_{r_0} as a function of the topological charge of the central vortex line s . v_{r_0} is the self-induced speed of a vortex ring with $R_r = 3$. **e** Relative translational speed v_{rl}/v_r as a function of the vortex ring radius R_r . v_r is the self-induced speed of a vortex ring with different radius R_r . **f** The initial Density cross sections along x for the three cases shown in (a). **g** The relative speed of the vortex ring as a function of the peak density of the system with respect to $s = 0, 1, \dots, 4$, $c = 0, 10, \dots, 40$, and the number of atoms $N_0 = 5.0 \times 10^5, 5.1 \times 10^5, \dots, 5.4 \times 10^5$. In **d**, **e**, and **g**, dashed lines connect markers via linear interpolation to show velocity trends.

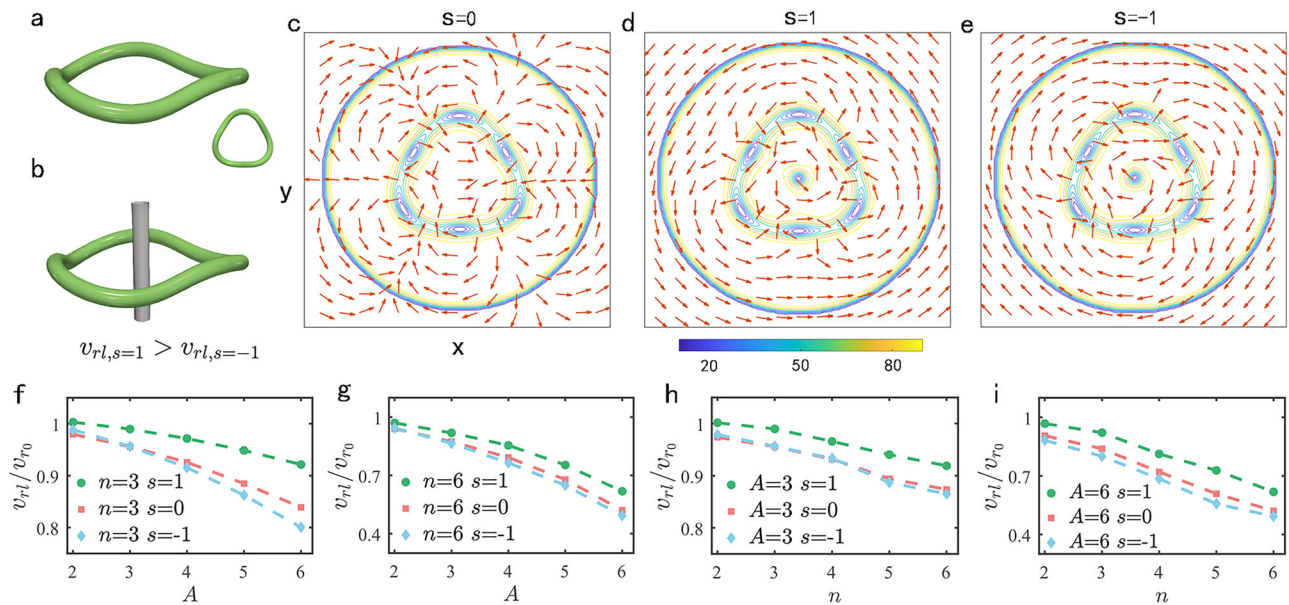


Fig. 2 | Translational dynamics of helical vortex rings. **a** The density isosurface of a helical vortex ring with the Kelvin wave number $n = 3$, and amplitude $A = 3$. The subplot is the top view of the helical vortex ring. **b** The density isosurface of the helical vortex ring in **a** with a $s = \pm 1$ vortex line at the center of the area enclosed by the ring. The initial speed field distributions on the (x, y) -plane of the helical ring **c** without vortex line, **d** with a topological charge $s = 1$ vortex line, and **e** with a $s = -1$

vortex line. **f** The ratio between the translational speed v_{rl} of the helical ring and the translational speed v_0 of the corresponding circular ring as a function of the Kelvin wave amplitude A for **f** $n = 3$, **g** $n = 6$. The relative speed v_{rl}/v_0 as a function of the Kelvin wave number n **h** for $A = 3$, and **i** $A = 6$. In **f**–**i**, dashed lines connect the markers to indicate velocity trends.

To gain further insights into the underlying cause of the increase in the translational speed, we compare the dynamics of the vortex ring under three distinct scenarios: a simple ring, a ring combined with a central vortex line, and a ring with a central Gaussian impurity. The Gaussian impurity $V_g = B \exp[-(x)^2 - (y)^2]/2c^2$ sitting at the center of the region enclosed by the vortex creates a void at the center of the condensate, where $B = 1000$ and c are the amplitude and the half-width of the Gaussian function, respectively. In Fig. 1a, we also present the density isosurfaces of the vortex structure with Gaussian impurities of $c = 10$ in green and $c = 30$ in pink. The initial positions of the vortex rings combined with Gaussian impurities align with the gray-colored vortex ring that contains a central vortex line. The corresponding speed field of the vortex ring with a $c = 10$ Gaussian impurity is shown in Fig. 1c, which is quite different from the speed field shown in Fig. 1b. The density distributions across the cross-section along the x -axis of the three scenarios are shown in Fig. 1f. In Fig. 1a, we can see clearly that with the same initial position, at $t = 8$, the translational speed of the vortex ring with a vortex line is larger than that of the vortex ring with Gaussian impurities. We see that the background density of the condensate undergoes changes in the presence of a vortex line or a Gaussian impurity while keeping the total number of atoms a constant. In Fig. 1g, we demonstrate the relative speed of the vortex ring as a function of the peak density ρ_0 of the condensate. Moreover, the presence of a Gaussian well can also lead to an increase in the speed of the vortex ring. However, we observe that to achieve the same increase in speed, the cavity created by the Gaussian potential (red dotted line in Fig. 1f) should be larger than the counterpart created by the correspondent vortex line. This indicates that the increase in the speed of the vortex ring depends on the shape of the density dip of the condensate, which subsequently alters the distribution of the speed field associated with the vortex ring. Moreover, in many experimental scenarios, highly charged vortex lines exhibit instability within the condensate^{40,41}. Nevertheless, the splitting of these vortex lines has little effect on the influence of their topological charge on the speed of the vortex ring (further details are provided in Fig. S1). Moreover, the introduction of multiple randomly positioned vortex lines can lead to a heightened speed of the vortex ring, with the extent of the speed enhancement contingent upon the arrangement of the vortex lines (detailed information is available in Fig. S2).

Helical vortex ring translational speed

We know that Kelvin waves can reduce the translational speed of a vortex ring^{42,43}. Now, we apply helical Kelvin waves on a vortex ring with radius R_r and initially positioned at z_0 in the z -axis. Then, a central vortex line is applied to see the combined effect of Kelvin waves and the line on the translational speed of the vortex ring. In Fig. 2a, we display the density isosurfaces of the vortex ring with wave number $n = 3$ and amplitude $A = 3$ Kelvin waves. Figure 2b displays the introduction of a central vortex line at the center of the area enclosed by the helical vortex ring. As the vortex ring encounters distortion from the Kelvin waves, the speed field surrounding the vortex ring no longer aligns perpendicularly with that surrounding the vortex line. The combination of the two speed fields can significantly change the motion of the vortex ring. The corresponding speed field distributions in the (x, y) -plane of the helical vortex ring without and with an $s = \pm 1$ vortex line are shown in Fig. 2c–e, where the influence of the vortex line on the flow speed field is prominently displayed. The flow speed field exhibits changes in both along the vortex line and around the vortex ring, which can be interpreted as twisting of the vortex⁴⁴. Helicity is a crucial conserved quantity in 3D ideal fluids (more details can be found in Eq. (S1)). However, due to the lack of internal structure in quantum vortex lines, the twisting component, a significant aspect of helicity, cannot be directly measured. As a result, exploring the twisting induced by the interaction between vortex lines and vortex rings presents an intriguing research opportunity^{45–48}.

Figure 2f–i demonstrates the significance of the topological charge polarity of the vortex line in this scenario. When A and n are small, the reduction in the vortex ring's speed caused by the Kelvin waves is minor and might be counterbalanced by the increase in speed due to the vortex line. Conversely, for larger values of A and n , a vortex line with a positive topological charge mitigates the reduction in speed, while a negative topological charge amplifies this effect. The mitigating effect of $s = 1$ surpasses the amplifying effect of $s = -1$ on the reduction in the vortex ring's speed. Considering a fixed Kelvin wave number n , the relative translational speed between the helical vortex ring with a central vortex line and the simple helical vortex ring decreases with an increase in the Kelvin waves' amplitude. Increased A values result in a more significant impact on either amplifying or alleviating the reduction in speed. Likewise, with a fixed amplitude A of

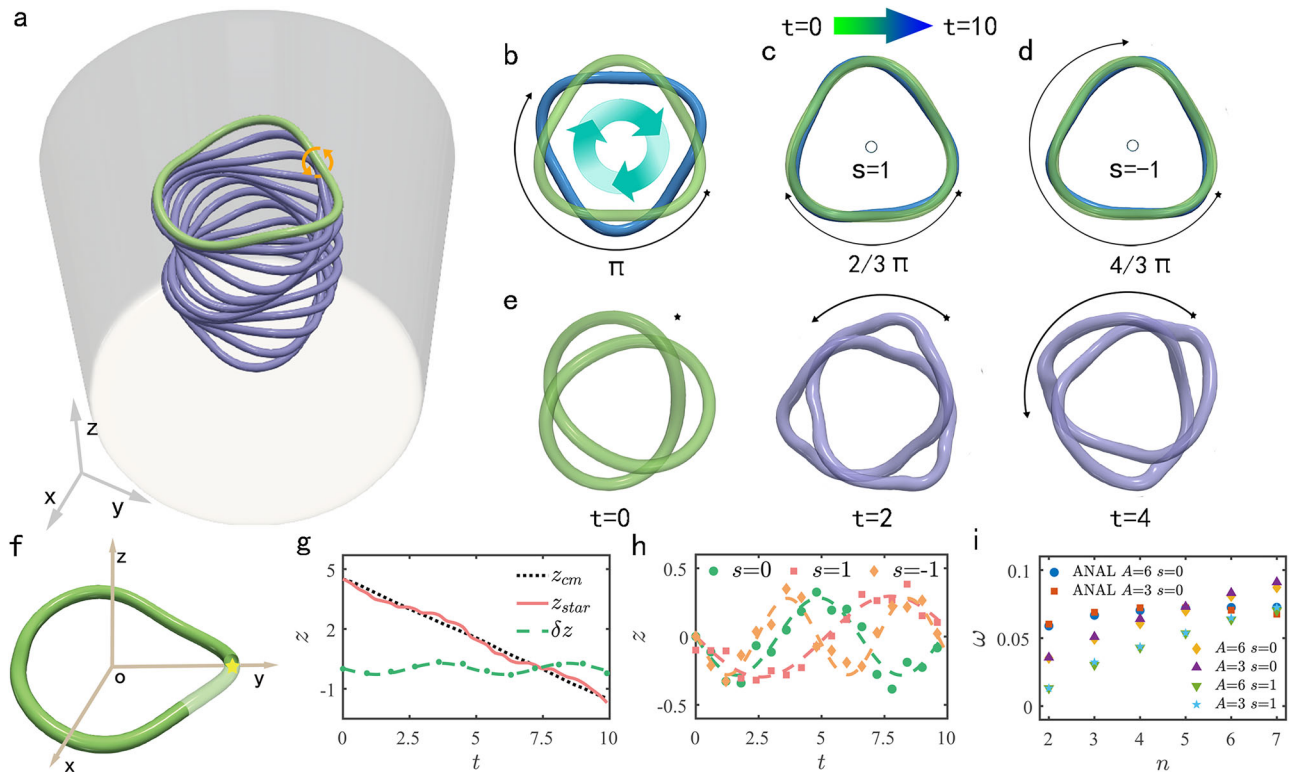


Fig. 3 | Rotational dynamics of helical vortices with the Kelvin wave number $n = 3$ and amplitude $A = 3$. **a** Snapshots of the time evolution of the helical vortex ring in a cylindrical trap. The original helical vortex ring is represented in green, while the subsequent dynamics in the series are depicted in purple. The circulation direction around the vortex is indicated by orange arrows. The density isosurfaces of the helical vortex ring at $t = 0$ (green) and $t = 10$ (blue) **b** without a central vortex line, **c** with a $s = 1$ central vortex line, and **d** with a $s = -1$ central vortex line. The light blue arrow marks the rotational direction of the helical vortex ring. The black pentagram and arrow mark the position of a point on the helical vortex ring at $t = 0$ and its corresponding position at $t = 10$, respectively. **e** The density isosurfaces of a trefoil at

$t = 0, 2$, and 4 . **f** Main view of a helical vortex ring with the yellow star indicating a 2D point vortex on the (y, z) -plane. **g** The z -component of the center of mass of the ring z_{cm} (black dotted line) and the position of the star in the z -direction z_{star} (red solid line) as a function of time t . The oscillatory behavior of the 2D point vortex δz (green dots) is obtained by subtracting z_{cm} from z_{star} , and then fitting it with a sine function (green dashed line). **h** The positional oscillation of the 2D point vortex in the z -direction with vortex lines carrying different topological charges. The dashed line is obtained by fitting the oscillatory behavior with a sine function. **i** The rotation frequency of the vortex ring, $\omega = 2\pi\omega_v/n$, as a function of the Kelvin wave number n , where ANAL denotes the analytical result.

Kelvin waves, the relative translational speed diminishes with escalating n . It is noted that for more substantial perturbations, there may be a possibility of connection between the vortex line and the vortex ring²⁷.

Helical vortex ring angular rotation

Now, we will explore the impact of Kelvin waves on the rotational motion of a vortex ring. Figure 3a exhibits sequential snapshots of a helical vortex ring at various time intervals in a homogeneous background (refer to Supplementary Movie 1). The ring maintains a relatively consistent shape throughout its evolution, enabling its treatment as a rigid structure. The vortex ring uniformly moves in the z -direction while rotating clockwise in the (x, y) -plane at a constant angular speed. In Fig. 3b–d, we illustrate the rotational dynamics of a helical vortex ring both without and with a central vortex line. From $t = 0$ to $t = 10$, the single helical vortex ring, without a central vortex line, undergoes a clockwise rotation around the z -axis by approximately π . However, the presence of a central vortex line alters the rotational motion of the vortex ring around the z -axis. In contrast to translational speed of a circular vortex ring, which is influenced solely by the absolute value of the topological charge of the vortex line, the rotation of the helical vortex ring is impacted by both the sign and strength of the topological charge of the vortex line. With a topological charge of $s = 1$, the rotational effect is weakened because the flow induced by the vortex line and the projection of the flow generated by the vortex ring onto the (x, y) -plane are in opposing directions. Conversely, when $s = -1$, the rotational effect is enhanced as the directions of the two flows align. For a more intricate structure like a trefoil, the rotational motion is also identifiable. However, its

shape undergoes variation due to self-interactions between different parts. Figure 3e depicts three snapshots illustrating the dynamics of a trefoil.

The helical vortex ring intersects the (y, z) -plane at two different points, which corresponds to two two-dimensional (2D) point vortices on the (y, z) -plane³⁸. The rotational behavior of the helical vortex ring, given its rigid characteristics, can be equivalently described as the oscillation of a 2D point vortex (marked by the yellow star on the (y, z) -plane in Fig. 3f) within the comoving frame. This frame moves in the $-z$ direction at a speed equal to the intrinsic translational speed of the vortex ring. In Fig. 3g, we illustrate the oscillatory nature of the 2D point vortex, denoted by the green dashed line. This representation is derived by tracking its movement (red solid line) and subsequently deducting the center-of-mass motion of the vortex ring (black dotted line). Additionally, we display the oscillatory patterns of a 2D point vortex in scenarios both with and without a central vortex line in Fig. 3h. Moreover, all the numerical findings align closely with sine functions. The frequency of oscillation of the 2D point vortex serves as an efficient method for determining the rotation frequency of the vortex ring $\omega = 2\pi\omega_v/n$. The observation that the oscillation frequency of the 2D point vortex in the presence of a vortex line with $s = -1$ surpasses that of the 2D point vortex accompanied by a vortex line with $s = 1$ aligns with the earlier conclusion depicted in Fig. 3c, d.

The oscillation frequency ω of the 2D point vortex can be influenced by factors such as the wave number n and amplitude A of the Kelvin waves, and the topological charge s of the central vortex line. Figure 3i presents ω as a function of n for various combinations of A and s . When A is much smaller than the vortex ring radius R_r , we can use the canonical relation of the

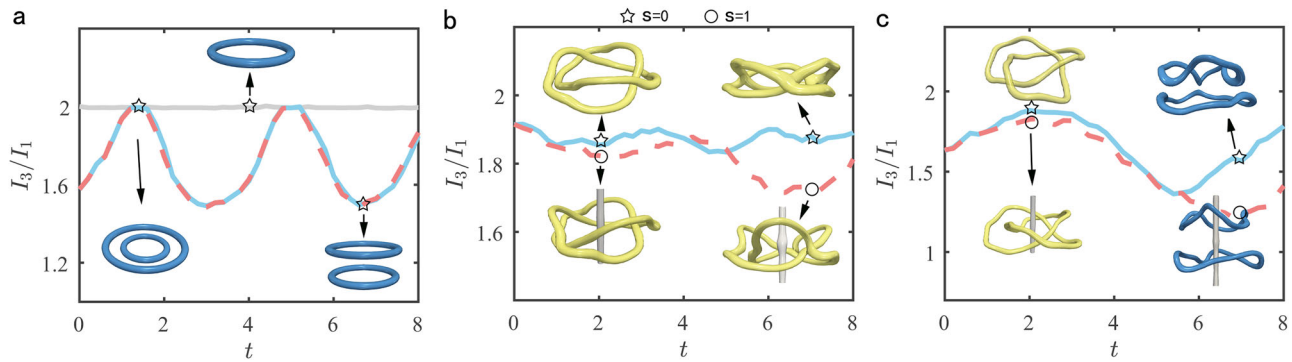


Fig. 4 | Time evolution of the transverse-to-vertical ratio of the vortex structures. **a** The transverse-to-vertical ratio as a function of time for a vortex ring (gray solid line), two coaxial vortex rings initially in the same plane (blue solid line), and the two vortex rings with a $s = 1$ central vortex line (red dashed line). During the dynamic process, the shape of the single ring remains unchanged, while the double rings undergo leapfrogging motion. For two vortex rings, the initial radii and the minimal distance of the upper and lower ring are $R_u = 2.0$, $R_l = 2.3$, and $d_{\min} = 1.5$, respectively. **b** The time evolution of the transverse-to-vertical ratio of a trefoil initially generated by phase imprinting with (red dashed line) and without (blue solid line) a $s = 1$ central vortex line. The toroidal and poloidal radii of the trefoil are $R_t = 2.0$ and

$R_p = 0.4$, respectively. During the dynamic process, the trefoil structure is well preserved. **c** Time evolution of the transverse-to-vertical ratio of two initial helical vortex rings with (red dashed line) and without (blue solid line) a $s = 1$ central vortex line. During the dynamic process, the two helical rings reconnect into a trefoil, which then breaks into two helical rings again. For two perturbed rings, the initial radii and the minimal distance of the upper and lower ring are $R_u = 2.0$, $R_l = 2.3$, and $d_{\min} = 1.0$, respectively. The radial and axial amplitudes of the Kelvin waves of the upper ring are $A_{xyu} = 0.8$ and $A_{zu} = 0.3$ and that of the lower ring are $A_{xyl} = 0.4$ and $A_{zl} = 0.2$, respectively. The initial relative angle and wave number of the rings are $\alpha = \pi/3$ and $n = 3$.

Hamiltonian equations of motion to analytically obtain the rotational frequency of the helical vortex ring in the local-induction approximation²¹:

$\omega = 2\pi\nu n / (R_c^2 \sqrt{1 + n^2(A/R_c)^2})$, where $\nu = \kappa \ln(\sqrt{R_c^2 + n^2 A^2} / nr_c) / 4\pi$ represents the line tension parameter, $\kappa = h/m$ signifies the circulation quantum, and r_c denotes the core radius. When the wave number of Kelvin waves is small, both numerical and analytical results suggest that the effect of A on ω can be disregarded. Our numerical findings illustrate that ω increases with rising n , while the analytical results suggest a decrease in ω for large n . We posit that the analytical results may not be applicable for large n . We noticed that both helical and straight vortex lines exert a comparable influence on the dynamics of circular vortex rings and helical vortex rings (detailed information is available in Fig. S3).

In our study, we aimed to evaluate the dynamic stability of the system by introducing 5% random perturbations into the initial wave function. Our results indicate that the helical vortex ring can keep its shape for small wave number of Kelvin waves within the time period studied. For high wave numbers of Kelvin waves, significant distortion occurs on both the vortex ring and the vortex line, leading to their connection. This disrupts the hopfion structure and extends the system beyond the scope of our study.

Vortex structure dynamics with vortex lines

We further examine the impact of a vortex line on the dynamics of more complex topological configurations, such as vortex trefoils and vortex links. The characteristics of these vortices can be measured through the assessment of their length, energy, and helicity^{2,23}. When the vortex formation loses its rigidity, additional characterization can be provided by the moment of inertia tensor. The ratio of transverse-to-vertical dimensions of the vortex structure can be deduced by computing the moment of inertia tensor elements. For this purpose, we introduce relative coordinates as $r_1 = x - x_{\text{cm}}$, $r_2 = y - y_{\text{cm}}$, $r_3 = z - z_{\text{cm}}$, where $(x_{\text{cm}}, y_{\text{cm}}, z_{\text{cm}})$ is the center of mass coordinate of the vortex structure. The relative moment of inertia tensor \mathbf{I} is defined as⁴⁹

$$\mathbf{I}_{ij} = \delta_{ij} \int M r^2 d\mathbf{r} - \int M r_i r_j d\mathbf{r}, \quad i, j = 1, 2, 3 \quad (3)$$

where $M = (\rho_{\text{th}} - |\psi|^2)H[\rho_{\text{th}} - |\psi|^2]$. By diagonalizing the matrix \mathbf{I} through an orthogonal transformation represented by \mathbf{U} , we obtain $\mathbf{U}\mathbf{I}\mathbf{U}^T = \text{diag}(I_1, I_2, I_3)$. Specifically, in our current setup, $I_3 = I_{33}$ with $I_3 > I_1 = I_2$. The ratio I_3/I_1 serves as an indication of the transverse-to-vertical

ratio of the vortex structure. For ellipsoids, the scenario where $I_3 > I_1 = I_2$ corresponds to an oblate ellipsoid, while the special case $I_3/2 = I_1 = I_2$ characterizes a flat disk without thickness.

In Fig. 4, we illustrate the temporal evolution of the transverse-to-vertical ratio, I_3/I_1 , for different vortex configurations. Figure 4a depicts the real-time transverse-to-vertical ratio for a simple vortex ring (the gray solid line), two coaxial vortex rings (the blue solid line), and a vertical vortex line encircled by two vortex rings (the red dashed line). It can be observed that the transverse-to-vertical ratio remains constant throughout the evolution of a single ideal vortex ring. Conversely, in the scenario of two coaxial vortex rings, the transverse-to-vertical ratio exhibits periodic oscillations, indicative of a traditional leapfrog motion. This motion initiates with the rear ring contracting radially and increasing in speed, while the front ring expands and decreases in speed simultaneously¹⁵. As the rear ring precisely transits through the leading ring, the two rings align in the same plane, resulting in identical transverse-to-vertical ratios for both the coaxial rings and the single ring. Furthermore, it is worth noting that the central vortex line exerts a slight influence on the leapfrog motion.

The vortex trefoil stands as the most elementary non-trivial knot. In Fig. 4b, the blue solid line portrays the temporal progression of the transverse-to-vertical ratio for a vortex trefoil. While the trefoil structure is intact, the transverse-to-vertical ratio undergoes slight oscillations. Introducing a vortex line decelerates the motion of the trefoil and amplifies the amplitude variation of the transverse-to-vertical ratio due to the significant deformation of the trefoil in the z -direction, as shown by the red dashed line. Additionally, considering that a trefoil can be formed by connecting two perturbed coaxial vortex rings converging towards each other²³, and the reverse process has been observed in both superfluids and normal fluids^{1,2,50}, we investigate the temporal evolution of the transverse-to-vertical ratio initiated by two helical vortex rings in Fig. 4c. The ratio increases until the two rings unite to form a trefoil through reconnection. Upon reaching a minimum ratio, the trefoil disintegrates back into two separate rings. The presence of a vortex line accentuates the deformation of the vortex structure in the z -direction, leading to a further reduction in the speed of the vortex motion.

In conclusion, our study delves into the dynamics of helical vortex rings. Our investigations reveal the ability to influence both the translational and rotational motion of a helical vortex ring through the incorporation of a vortex line. In the absence of Kelvin waves, the inclusion of a vortex line results in an increase in speed of a pristine vortex ring, disregarding the topological charge polarity of the line. Concerning helical vortex rings, the

reduction in speed caused by Kelvin wave perturbations can be augmented or diminished by the vortex line, contingent upon the topological charge polarity carried by the line. By leveraging the topological charge of the vortex line, along with the wave number and amplitude of the Kelvin waves, one can influence the translational dynamics of a vortex ring. Intriguingly, an alteration in the translational speed of the ring can be achieved by creating a cavity within the region enclosed by the vortex ring. The configuration of the aperture influences the translational motion, underscoring the significance of the speed field distribution surrounding a vortex ring on its movement.

Our analysis extends to the examination of the rotational behavior of helical vortex rings prompted by Kelvin waves. We discover that helical wave disturbances can induce rotation in the vortex ring, analogous to a similar phenomenon observed in a trefoil knot. The rotation frequency of a vortex ring can be deduced from the oscillation frequency of 2D point vortices along the ring. Moreover, we illustrate that the rotational motion can be influenced by adjusting the topological charge of a vortex line. When the flow direction of the vortex line aligns with that of the vortex ring, the rotational effect is enhanced; conversely, when they are in opposition, the rotational effect is diminished. These results enhance comprehension of the interplay among different vortex structures, aiding in the understanding of quantum turbulence within intricate systems. For instance, the random emission and collision of vortex rings can initiate a localized vortex tangle within the condensate, dynamically releasing vortex rings as part of the turbulence decay⁵¹. Furthermore, the interaction between vortex rings and vortex lines can cause deflections and changes in speed of vortex rings, as well as the generation of Kelvin waves and phonon excitations⁵². A comprehensive understanding of vortex ring dynamics and their interactions with vortex lines is imperative. To further elucidate the dynamics of complex vortex structures, we calculated the moment of inertia tensor to represent the transverse-to-vertical ratio of these structures. This provides a potential tool for analyzing the dynamics of complex vortices. We note that the density and phase of the superfluid wave function can be readily correlated with the density and speed in classical hydrodynamic fluids through the Madelung transform. The dynamics of vortex rings show similarities in both BECs and water^{37,53}. Consequently, our findings are valuable for elucidating phenomena in classical fluids.

Methods

Dimensionless process

To ensure both convenience and accuracy, we work with dimensionless parameters throughout our calculations. Vortex structures are created within the homogeneous background of the condensate using phase imprinting and imaginary time evolution techniques. Our simulations are conducted in a uniformly discrete computational domain with grid points $N_x \times N_y \times N_z = 151 \times 151 \times 151$, spatial resolution $\Delta x = \Delta y = \Delta z = \sqrt{2}a_0/10$, and reflective boundary conditions. To ensure the precision of solving the dimensionless GP equations, we employ both the Crank-Nicolson method and the fourth-order Runge-Kutta method, which consistently produce reliable results.

It is customary to scale the GP equation to a dimensionless form by using units of length, time, and energy are $a_0 = \sqrt{\hbar/2m\omega_0}$, $t_0 = 1/\omega_0$, and $E_0 = \hbar\omega_0$, respectively, where we choose $\omega_0 = 2\pi \times 75$ Hz as the reference frequency. The dimensionless GP equation then becomes

$$i \frac{\partial \psi}{\partial t} = \left[-\nabla^2 + V_{\text{trap}}(x, y, z) + U_0 |\psi|^2 \right] \psi \quad (4)$$

where $U_0 = 8\pi a_s \sqrt{2m\omega_0/\hbar}$ is the dimensionless interaction constant. The s-wave scattering length is $a_s = 5.4$ nm and the mass $m = 1.443 \times 10^{-25}$ kg for ⁸⁷Rb BECs. The system is trapped in a cylindrical box potential V_{trap} as

$$V_{\text{trap}}(x, y, z) = \begin{cases} 0, & r < 7 \text{ and } -7 \leq z \leq 7 \\ V_0, & \text{otherwise} \end{cases} \quad (5)$$

where $r = \sqrt{x^2 + y^2}$ and $V_0 = 300$ is the potential height.

Initial state construction

The initial states are constructed by introducing a lying vortex ring and a vertical straight vortex line that pierces through the center of the ring. The vortex rings can be perturbed by Kelvin waves characterized by different wave numbers and amplitudes. In experimental setups, initial vortices are typically created using phase imprinting techniques. In numerical simulations, the initial state is achieved by evolving the GP equation in imaginary time with the initial wave function. A reasonable assumption for the initial wave function of a helical vortex ring and a vortex line is given by³⁸

$$\begin{aligned} \psi_{3D}(x, y, z) = & \psi_{2Dr} \{ r - R_r - A \sin[n\theta(x, y)], \\ & z - z_0 - A \cos[n\theta(x, y)] \} \times \\ & \psi_{2Dr}^* \{ r + R_r - A \sin[n\theta(-x, -y)], \\ & z - z_0 - A \cos[n\theta(-x, -y)] \} \times \\ & \psi_{2Dl}(x, y) \end{aligned} \quad (6)$$

where $\psi_{2Dr}(r, z) = \sqrt{N_0} \exp[i\theta(r, z)]$, $\psi_{2Dl}(x, y) = \sqrt{N_0} \exp[is\theta(x, y)]$, $\theta(x, y) = \text{atan2}(y, x)$, N_0 is the total number of atoms, s is the topological charge of the vortex line, z_0 is the initial position of the center of mass of the helical ring along the z -axis, A and n are the amplitude and the wave number of Kelvin waves, respectively. The initial wave function provides a phase θ , from which the speed field of the condensate can be determined as $v = \hbar/m \nabla \theta$. The helical vortex rings generated in the main text rotate clockwise, whereas the initial wave function of counterclockwise rotating vortex rings can be found in Fig. S4 and Eq. (S2).

In our plots, we define iso-surfaces by selecting a threshold density based on a constant value proportional to the maximum density. Specifically, we choose a threshold density value that is about 20% of the peak density within the system, consistent with the approach in ref. 38. This guarantees that the iso-surfaces accurately represent the essential structural characteristics of the vortex, excluding low-density areas that have minimal impact on the overall dynamics. To study the influence of a central vortex line on the dynamics of a vortex ring, it is necessary to maintain the hopfion structure by employing two key strategies. These strategies are designed to preserve the geometric integrity necessary for analyzing how the central vortex line affects the behavior of the vortex ring. Firstly, we meticulously positioned the vortex line along the axis of the vortex ring. Secondly, we ensure that the size of the background condensate, determined by the radius of the cylindrical trap, is at least double the radius of the vortex ring. This approach effectively maintains a sufficient distance between the vortex line, vortex ring, and the boundary of the system. Improper selection of initial parameters, as illustrated in Figs. S1 and S2, may result in the splitting of the vortex line, tilting of the vortex ring, or even the reconnection of the vortex line with the vortex ring. Such deviations may significantly impact the influence of the vortex line on the velocity of the vortex ring.

Data availability

The data that support the findings of this study are available from the corresponding author upon reasonable request.

Code availability

The code used in this study is available from the corresponding author upon reasonable request.

Received: 29 April 2024; Accepted: 23 April 2025;

Published online: 29 April 2025

References

- Kleckner, D. & Irvine, W. T. M. Creation and dynamics of knotted vortices. *Nat. Phys.* **9**, 253–258 (2013).
- Kleckner, D., Kauffman, L. H. & Irvine, W. T. M. How superfluid vortex knots untie. *Nat. Phys.* **12**, 650 (2016).
- Qi, Y. et al. Fragmentation in turbulence by small eddies. *Nat. Commun.* **13**, 469 (2022).

4. Cummins, C. et al. A separated vortex ring underlies the flight of the dandelion. *Nature* **562**, 414 (2018).
5. Pulvirenti, F., Scollo, S., Scollo, S. & Schwandner, F. M. Dynamics of volcanic vortex rings. *Sci. Rep.* **1**, 2369 (2023).
6. Dennis, M. R., King, R. P., Jack, B., O' Holleran, K. & Padgett, M. J. Isolated optical vortex knots. *Nat. Phys.* **6**, 118–121 (2010).
7. Tempone-Wiltshire, S. J., Johnstone, S. P. & Helmersson, K. Optical vortex knots - one photon at a time. *Sci. Rep.* **6**, 24463 (2016).
8. Jackson, B., McCann, J. F. & Adams, C. S. Vortex line and ring dynamics in trapped Bose-Einstein condensates. *Phys. Rev. A* **61**, 013604 (1999).
9. Minowa, Y. et al. Visualization of quantized vortex reconnection enabled by laser ablation. *Sci. Adv.* **8**, eabn1143 (2022).
10. Wang, W., Kolokolnikov, T., Frantzeskakis, D. J., Carretero-González, R. & Kevrekidis, P. G. Pairwise interactions of ring dark solitons with vortices and other rings: stationary states, stability features, and nonlinear dynamics. *Phys. Rev. A* **104**, 023314 (2021).
11. Maucher, F., Skupin, S., Gardiner, S. A. & Hughes, I. G. Creating complex optical longitudinal polarization structures. *Phys. Rev. Lett.* **120**, 163903 (2018).
12. Maucher, F., Gardiner, S. A. & Hughes, I. G. Excitation of knotted vortex lines in matter waves. *New J. Phys.* **18**, 063016 (2016).
13. Boullé, N., Newell, I., Farrell, P. E. & Kevrekidis, P. G. Two-component three-dimensional atomic Bose-Einstein condensates supporting complex stable patterns. *Phys. Rev. A* **107**, 012813 (2023).
14. Pan, L., Zhu, X., Zhu, Q.-L., Liu, Y. & An, J. Dynamics of a vortex ring encountering a spherical obstacle in Bose-Einstein condensates. *Phys. Rev. A* **105**, 033313 (2022).
15. Niemi, A. J. Exotic statistics of leapfrogging vortex rings. *Phys. Rev. Lett.* **94**, 124502 (2005).
16. Khani, K. et al. Critical transport and vortex dynamics in a thin atomic Josephson junction. *Phys. Rev. Lett.* **124**, 045301 (2020).
17. Villosio, A., Proment, D. & Krstulovic, G. Irreversible dynamics of vortex reconnections in quantum fluids. *Phys. Rev. Lett.* **125**, 164501 (2020).
18. Anderson, B. P. et al. Watching dark solitons decay into vortex rings in a Bose-Einstein condensate. *Phys. Rev. Lett.* **86**, 2926–2929 (2001).
19. Bai, W.-K., Xing, J.-C., Yang, T., Yang, W.-L. & Liu, W.-M. Nonlinear dynamics of a Bose-Einstein condensate excited by a vortex ring phase imprinting. *Results Phys.* **22**, 103828 (2021).
20. Helm, J. L., Barenghi, C. F. & Youd, A. J. Slowing down of vortex rings in Bose-Einstein condensates. *Phys. Rev. A* **83**, 045601 (2011).
21. Sonin, E. B. Dynamics of helical vortices and helical-vortex rings. *EPL* **97**, 46002 (2012).
22. Scheeler, M. W., van Rees, W. M., Kedia, H., Kleckner, D. & Irvine, W. T. M. Complete measurement of helicity and its dynamics in vortex tubes. *Science* **357**, 487–491 (2017).
23. Bai, W.-K., Yang, T. & Liu, W.-M. Topological transition from superfluid vortex rings to isolated knots and links. *Phys. Rev. A* **102**, 063318 (2020).
24. Kartashov, Y. V., Malomed, B. A., Shnir, Y. & Torner, L. Twisted toroidal vortex solitons in inhomogeneous media with repulsive nonlinearity. *Phys. Rev. Lett.* **113**, 264101 (2014).
25. Bidasyuk, Y. M. et al. Stable Hopf solitons in rotating Bose-Einstein condensates. *Phys. Rev. A* **92**, 053603 (2015).
26. Bisset, R. N. et al. Robust vortex lines, vortex rings, and hopfions in three-dimensional Bose-Einstein condensates. *Phys. Rev. A* **92**, 063611 (2015).
27. Zou, S., Bai, W.-K., Yang, T. & Liu, W.-M. Formation of vortex rings and hopfions in trapped Bose-Einstein condensates. *Phys. Fluids* **33**, 027105 (2021).
28. Baggaley, A. W. & Barenghi, C. F. Spectrum of turbulent kelvin-waves cascade in superfluid helium. *Phys. Rev. B* **83**, 134509 (2011).
29. Laurie, J. & Baggaley, A. W. A note on the propagation of quantized vortex rings through a quantum turbulence tangle: energy transport or energy dissipation? *J. Low Temp. Phys.* **180**, 95 (2015).
30. Kursa, M., Bajer, K. & Lipniacki, T. Cascade of vortex loops initiated by a single reconnection of quantum vortices. *Phys. Rev. B* **83**, 014515 (2011).
31. Barenghi, C. F., Middleton-Spencer, H. A. J., Galantucci, L. & Parker, N. G. Types of quantum turbulence. *AVS Quantum Sci.* **5**, 025601 (2023).
32. Green, P. J., Grant, M. J., Nevin, J. W., Walmsley, P. M. & Golov, A. I. Quantized vortex rings and loop solitons. *J. Low Temp. Phys.* **201**, 11 (2020).
33. Galantucci, L., Krstulovic, G. & Barenghi, C. F. Friction-enhanced lifetime of bundled quantum vortices. *Phys. Rev. Fluids* **8**, 014702 (2023).
34. Nakagawa, T., Inui, S. & Tsubota, M. Internal structure of localized quantized vortex tangles. *Phys. Rev. B* **104**, 094510 (2021).
35. Galantucci, L., Rickinson, E., Baggaley, A. W., Parker, N. G. & Barenghi, C. F. Dissipation anomaly in a turbulent quantum fluid. *Phys. Rev. Fluids* **8**, 034605 (2023).
36. Roberts, P. H. & Grant, J. Motions in a Bose condensate. I. The structure of the large circular vortex. *J. Physica A* **4**, 55 (1971).
37. Matsuzawa, T., Mitchell, N. P., Perrard, S. & Irvine, W. T. M. Creation of an isolated turbulent blob fed by vortex rings. *Nat. Phys.* **19**, 1193 (2023).
38. Proment, D., Onorato, M. & Barenghi, C. F. Vortex knots in a Bose-Einstein condensate. *Phys. Rev. E* **85**, 036306 (2012).
39. Foster, C. J., Blakie, P. B. & Davis, M. J. Vortex pairing in two-dimensional Bose gases. *Phys. Rev. A* **81**, 023623 (2010).
40. Wang, W. et al. Single and multiple vortex rings in three-dimensional Bose-Einstein condensates: existence, stability, and dynamics. *Phys. Rev. A* **95**, 043638 (2017).
41. Bisset, R. N. et al. Bifurcation and stability of single and multiple vortex rings in three-dimensional Bose-Einstein condensates. *Phys. Rev. A* **92**, 043601 (2015).
42. Barenghi, C. F., Hänninen, R. & Tsubota, M. Anomalous translational velocity of vortex ring with finite-amplitude Kelvin waves. *Phys. Rev. E* **74**, 046303 (2006).
43. Hershberger, R. E., Bolster, D. & Donnelly, R. J. Slowing of vortex rings by development of Kelvin waves. *Phys. Rev. E* **82**, 036309 (2010).
44. Radu, E. & Volkov, M. S. Stationary ring solitons in field theory — knots and vortons. *Phys. Rep.* **468**, 101–151 (2008).
45. Salman, H. Helicity conservation and twisted Seifert surfaces for superfluid vortices. *Proc. R. Soc. A* **473**, 20160853 (2017).
46. Zuccher, S. & Ricca, R. L. Twist effects in quantum vortices and phase defects. *Fluid Dyn. Res.* **50**, 011414 (2018).
47. Foresti, M. & Ricca, R. L. Defect production by pure phase twist injection as Aharonov-Bohm effect. *Phys. Rev. E* **100**, 023107 (2019).
48. Foresti, M. & Ricca, R. L. Hydrodynamics of a quantum vortex in the presence of twist. *J. Fluid Mech.* **904**, A25 (2020).
49. Hand, L. N. & Finch, J. D. *Analytical Mechanics* (Cambridge University Press, 1998).
50. Zuccher, S. & Ricca, R. L. Creation of quantum knots and links driven by minimal surfaces. *J. Fluid Mech.* **942**, A8 (2022).
51. Nakagawa, T., Inui, S., Tsubota, M. & Yano, H. Statistical laws and self-similarity of vortex rings emitted from a localized vortex tangle in superfluid ⁴He. *Phys. Rev. B* **101**, 184515 (2020).
52. Villosio, A., Salman, H. & Proment, D. Scattering of line-ring vortices in a superfluid. *J. Low Temp. Phys.* **180**, 68 (2015).
53. Barenghi, C. F. & Donnelly, R. J. Vortex rings in classical and quantum systems. *Fluid Dyn. Res.* **41**, 051401 (2009).

Acknowledgements

We thank Renzo Ricca, Jun-Hui Zheng, Wen-Long Wang, Chen Jiao and Han-Jie Zhu for the helpful discussions. This work is supported by National Natural Science Foundation of China under grants Nos. 12305029, 12247186, 12175180, 12247103, 12174461, 12234012, 12334012, and 52327808, the Natural Science Basic Research Program of Shaanxi under grants No. 2023-JC-QN-0054, Shaanxi Fundamental Science Research Project for Mathematics and Physics under grants No. 22JSZ005, the Youth Innovation Team of Shaanxi Universities, National Key R&D Program of China under grants

Nos. 2021YFA1400900, 2021YFA0718300, 2021YFA1402100, and Space Application System of China Manned Space Program.

Author contributions

W.-K.B. and X.Y. conducted numerical simulations and prepared the paper under the guidance of T.Y., S.A.G. and W.-M.L. H.Z. provided theoretical and numerical expertise. W.-K.B. and T.Y. contributed to the discussion regarding paper enhancements. All authors participated in result discussions, analyzed dynamic mechanisms, and contributed to the revisions.

Competing interests

The authors declare no competing interests.

Additional information

Supplementary information The online version contains supplementary material available at

<https://doi.org/10.1038/s42005-025-02109-x>.

Correspondence and requests for materials should be addressed to S. A. Gardiner, Wu-Ming Liu or Tao Yang.

Peer review information *Communications Physics* thanks Davide Proment and the other, anonymous, reviewer(s) for their contribution to the peer review of this work.

Reprints and permissions information is available at <http://www.nature.com/reprints>

Publisher's note Springer Nature remains neutral with regard to jurisdictional claims in published maps and institutional affiliations.

Open Access This article is licensed under a Creative Commons Attribution-NonCommercial-NoDerivatives 4.0 International License, which permits any non-commercial use, sharing, distribution and reproduction in any medium or format, as long as you give appropriate credit to the original author(s) and the source, provide a link to the Creative Commons licence, and indicate if you modified the licensed material. You do not have permission under this licence to share adapted material derived from this article or parts of it. The images or other third party material in this article are included in the article's Creative Commons licence, unless indicated otherwise in a credit line to the material. If material is not included in the article's Creative Commons licence and your intended use is not permitted by statutory regulation or exceeds the permitted use, you will need to obtain permission directly from the copyright holder. To view a copy of this licence, visit <http://creativecommons.org/licenses/by-nc-nd/4.0/>.

© The Author(s) 2025